Wire-Length Dependence of the Conductance of Oligo(*p*-phenylene) Dithiolate Wires: A Consideration from Molecular Orbitals

Masakazu Kondo, Tomofumi Tada, and Kazunari Yoshizawa*

Institute for Materials Chemistry and Engineering, Kyushu University, Fukuoka 812-8581, Japan

Received: December 26, 2003; In Final Form: July 10, 2004

The electrical transmission of a series of oligo(*p*-phenylene) dithiolate (PDT) wires coupled with gold electrodes is investigated using a Green function method combined with a hybrid density functional method. To investigate how the nonplanarity of the π-backbone affects the electrical transmission, two types of PDT wires with planar and nonplanar forms are compared. The exponential decay of conductance at the Fermi level, $G(E_F) = G_0 \exp(-\gamma L)$, is observed for both forms. The damping factors, γ's, for the planar and nonplanar PDT wires are 0.165 and 0.256 Å^{-1}, respectively, these values being comparable with experimental data for analogous oligophenylene wires. A possible reason for the slower decay in the planar PDT wires is analyzed in terms of molecular orbitals.

Introduction

The development of nanotechnology enables us to manipulate nanosized molecules.[1−3] Molecules can be used as active components of electronic devices such as rectifiers and switches. Since understanding the electron transport through single molecules is essential toward molecular electronics, the electrical conduction through molecules has been experimentally measured using mechanically controllable break junction,[4−6] scanning tunneling microscopy,[7] and atomic force microscopy[8−10] techniques. Parallel to experiments, theoretical studies on quantum transport through atomic and molecular wires have been performed.[11−29] It is important to take the electronic structure of molecules in junctions into account in order to increase our understanding of quantum transport.

Oligo(*p*-phenylene) dithiolate (PDT), S−$(C_6H_4)_n$−S, is considered as a typical molecular wire. The electronic transport through benzene 1,4-dithiolate (BDT, $n = 1$) has been extensively investigated using various methods based on the Green function method.[17−26] Recently, density functional theory (DFT) is applied for the calculation of the transmission function of BDT coupled with gold electrodes within the framework of the Green function method.[21−26] Although some studies addressed the conductance properties of longer PDT wires from extended Hückel calculations,[17,27] the conductance of these long wires has not quantitatively been investigated with DFT.

In the present study, we investigate the quantum transport through a series of PDT wires shown in Figure 1 using a Green function method combined with a hybrid DFT method. A main purpose of this study is to shed new light on nonplanarity effects of the π-backbone on the conductance of the longer PDT systems. We first apply the method described below to the calculation of the electrical transmission through the BDT molecule to give a reasonable transmission function. We further study the electronic transport through the longer oligo(*p*-phenylene) dithiolate wires with planar and nonplanar forms. Previous studies[28,29] indicate that the magnitudes of the molecular orbital (MO) coefficients and the orbital phases, especially those of the highest occupied MO (HOMO) and the lowest unoccupied MO (LUMO), are important guidelines for understanding quantum transport properties of molecular wires. We see that the relationship between the HOMO and the conductance illuminates the importance of planarity for the effective quantum transport.

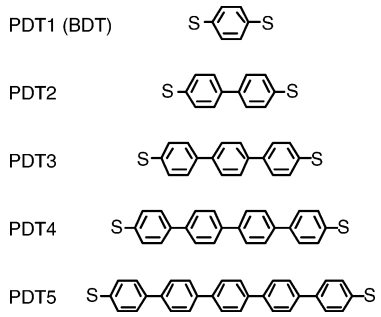

Figure 1. Oligo(*p*-phenylene) dithiolate (PDT) wires.

The rest of this paper is organized as follows. We describe the theoretical model and theoretical background in the next section. We give the method of choice in Computational Method and the transmission spectra for the PDT wires and some discussions in Results and Discussion. Finally, we end this manuscript by summarizing the results in Concluding Remarks.

Theoretical Background

A molecular junction is divided into three parts: left electrode (M_L), molecule (insulator, I), and right electrode (M_R) (MIM junction). Although in previous studies we took only the nearest-neighbor interaction between M and I into account,[28,29] multiple sites should be considered for more quantitative discussion. The extension to a multipath model shown in Figure 2 is straightforward. The retarded and advanced Green functions in the molecular part in this model are written as eq 1:

$$[\mathbf{G}^{R/A}(E)]_{ab} = [\mathbf{G}^{(0)R/A}(E)]_{ab} + \sum_{m,n\in M_L} [\mathbf{G}^{(0)R/A}(E)]_{am}[\Sigma_L^{R/A}(E)]_{mn}[\mathbf{G}^{R/A}(E)]_{nb} + \sum_{m',n'\in M_R} [\mathbf{G}^{(0)R/A}(E)]_{am'}[\Sigma_R^{R/A}(E)]_{m'n'}[\mathbf{G}^{R/A}(E)]_{n'b} \quad (1)$$

* To whom correspondence should be addressed. E-mail: kazunari@ms.ifoc.kyushu-u.ac.jp.

10.1021/jp038018u CCC: $27.50
Published on Web 09/24/2004

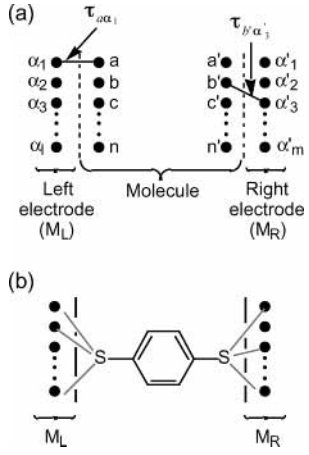

Figure 2. (a) Schematic representation of an MIM junction. The dashed lines represent the boundaries between electrodes and a molecule, and the shaded circles are contact points. Elements $\tau_{a\alpha}$ indicate the hopping integrals between "site *a*" of a molecule and the "site α" of an electrode. (b) Eight valence orbitals of each sulfur atom are included as sites in the molecular part.

where the self-energy matrix elements for the left and right electrodes are

$$[\Sigma_{\mathrm{L}}^{\mathrm{R/A}}(E)]_{mn} = \sum_{\alpha,\beta\in \mathrm{M_L}} \tau_{m\alpha}[\mathbf{g}_{\mathrm{L}}^{\mathrm{R/A}}(E)]_{\alpha\beta}\tau_{n\beta} \qquad (2)$$

and

$$[\Sigma_{\mathrm{R}}^{\mathrm{R/A}}(E)]_{m'n'} = \sum_{\alpha',\beta'\in \mathrm{M_R}} \tau_{m'\alpha'}[\mathbf{g}_{\mathrm{R}}^{\mathrm{R/A}}(E)]_{\alpha'\beta'}\tau_{n'\beta'} \qquad (3)$$

respectively. $\mathbf{g}_{\mathrm{L}}^{\mathrm{R/A}}$ and $\mathbf{g}_{\mathrm{R}}^{\mathrm{R/A}}$ are the Green functions of the left and right electrodes uncoupled with the molecule, respectively, and $\mathbf{G}^{(0)\mathrm{R/A}}$ is the zeroth-order Green function. The matrix elements of $\mathbf{G}^{(0)\mathrm{R/A}}$ are written as eq 4 on the basis of the MO scheme:[30]

$$[\mathbf{G}^{(0)\mathrm{R/A}}(E)]_{\alpha\beta} = \sum_m \frac{C_{m\alpha}C_{m\beta}}{E - \epsilon_m \pm \mathrm{i}\eta} \qquad (4)$$

where $C_{m\alpha}$ is the *m*th MO coefficient in atomic orbital (AO) α, ϵ_m is the *m*th MO energy of the molecule, and η is an infinitesimal constant. The self-energy matrices in this model are written in the block-diagonal form, as shown in

$$\Sigma^{\mathrm{R/A}}(E) = \begin{pmatrix} \Sigma_{\mathrm{L}}^{\mathrm{R/A}}(E) & \mathbf{0} \\ \mathbf{0} & \Sigma_{\mathrm{R}}^{\mathrm{R/A}}(E) \end{pmatrix} = \begin{pmatrix} \Sigma_{\mathrm{L}}^{\mathrm{R/A}}(E) & \mathbf{0} \\ \mathbf{0} & \mathbf{0} \end{pmatrix} + \begin{pmatrix} \mathbf{0} & \mathbf{0} \\ \mathbf{0} & \Sigma_{\mathrm{R}}^{\mathrm{R/A}}(E) \end{pmatrix} \equiv \underline{\Sigma}_{\mathrm{L}}^{\mathrm{R/A}}(E) + \underline{\Sigma}_{\mathrm{R}}^{\mathrm{R/A}}(E) \quad (5)$$

In the matrix form, eq 1 is rewritten as

$$\mathbf{G}^{\mathrm{R/A}}(E) = \mathbf{G}^{(0)\mathrm{R/A}}(E) + \mathbf{G}^{(0)\mathrm{R/A}}(E)\,\Sigma^{\mathrm{R/A}}(E)\,\mathbf{G}^{\mathrm{R/A}}(E) \quad (6)$$

and the Green function matrices for the molecular part of the MIM junction are given as

$$\mathbf{G}^{\mathrm{R/A}}(E) = [\mathbf{I} - \mathbf{G}^{(0)\mathrm{R/A}}(E)\,\Sigma^{\mathrm{R/A}}(E)]^{-1}\,\mathbf{G}^{(0)\mathrm{R/A}}(E) \qquad (7)$$

where **I** is the unit matrix. Using the Green function and self-energy matrices, the transmission functions are calculated through the following expression:[31]

$$T(E) = \mathrm{Tr}[\Gamma_{\mathrm{L}}(E)\,\mathbf{G}^{\mathrm{R}}(E)\,\Gamma_{\mathrm{R}}(E)\,\mathbf{G}^{\mathrm{A}}(E)] \qquad (8)$$

where Tr denotes the trace over all of the sites and where $\Gamma_{\mathrm{L}}(E)$ and $\Gamma_{\mathrm{R}}(E)$ correspond to $\mathrm{i}[\underline{\Sigma}_{\mathrm{L}}^{R}(E) - \underline{\Sigma}_{\mathrm{L}}^{\mathrm{A}}(E)]$ and $\mathrm{i}[\underline{\Sigma}_{\mathrm{R}}^{\mathrm{R}}(E) - \underline{\Sigma}_{\mathrm{R}}^{\mathrm{A}}(E)]$, respectively.

Computational Method

We considered the electrical transmission through the oligo(*p*-phenylene) dithiolate (PDT*n*, $n = 1-5$) wires in Figure 1 and the wire-length dependence of the conductance of these. We calculated the electronic structures of the PDT molecules with one additional gold atom on both sides of the sulfur atoms to ensure the lineup of the molecular levels relative to the Fermi level of the electrodes.[32] We used the B3LYP method[33,34] with the LANL2DZ basis set[35,36] for geometry optimizations and vibrational analyses on the Gaussian 98 code.[37] Then the Green function matrix elements of the molecules were obtained from eq 7 from MO coefficients and orbital energies calculated at the B3LYP/LANL2DZ level of theory. We took only the AOs of the sulfur atoms into account as interacting sites. Since each sulfur atom has eight split valence AOs, the dimension of the Green function matrices is 16. The reduction of the dimension of the Green function means that this computation is performed in a non-self-consistent treatment.

In the calculation of the Green function of the molecular part, it is necessary to obtain the self-energy matrix. We treated the self-energy matrices as adjustable parameters and obtained them as follows. The Green function of electrodes and hopping matrix elements are necessary in obtaining the self-energy matrix. We adopted the hopping integrals between the AOs of the gold and sulfur atoms as the molecule−electrode coupling elements in τ's. The extended Hückel method[38] implemented in the YAeHMOP package[39] was used to estimate the hopping matrix elements. In the extended Hückel calculation of a small cluster composed of a sulfur and three gold atoms, the nearest Au−Au distances and the Au−S bond lengths were set to be 2.88 Å, the value for bulk gold, and 2.40 Å, an optimized Au−S bond length at the B3LYP/LANL2DZ level of theory, respectively. We then multiplied the matrix elements by a scaling factor of 0.25. The Green function of Au(111) surface was calculated from the decimation technique[40,41] with the Slater−Koster two-center parameters.[42,43] For simplicity, we took only the diagonal elements of the Green functions of the electrodes into account. Taking small charge transfer between the molecules and the gold atom (less than 0.06*e*) into consideration,[32] the position of the Fermi level of the gold electrodes was fixed to be −5.31 eV, the work function of Au(111).[44]

We obtained reasonable transmission spectra for the BDT wire and other PDT wires using the present computational method. As shown below, computed dumping factors for the PDT system are comparable with experimental and other theoretical values. Furthermore, we applied the present computational procedure to another molecular wire and obtained a reasonable result.[45] The present computational scheme is useful for understanding quantum transport from the viewpoint of MOs.

Results and Discussion

Optimized Geometries of Molecular Wires. Let us consider three conformations in Figure 3 (P1, X1, and X2), in which the two gold atoms of P1 and X1 are located out of the benzene plane while X2 is planar. We optimized these three conformations at the B3LYP/LANL2DZ level of theory under C_i (for P1 and X1) and C_{2h} (for X2) symmetry. We found P1 to be 0.05

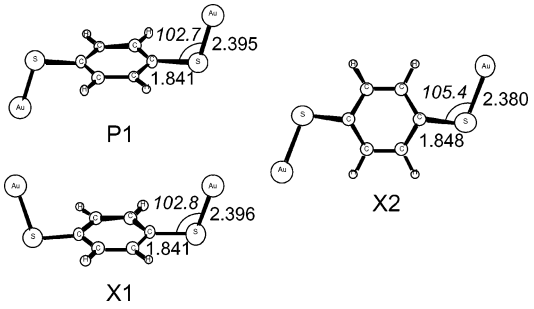

Figure 3. Extended molecules of benzene 1,4-dithiolate with different conformations of gold atoms. Bond lengths (plain) and bond angles (italic) are in angstroms and degrees, respectively.

and 6.02 kcal/mol more stable than X1 and X2, respectively. The energy difference between P1 and X2 is in good agreement with 5.75 kcal/mol obtained at the B3PW91/LANL2DZ level of theory.[23] We adopted the P1 conformation for all the PDT molecules. We also performed geometry optimizations for a BDT cluster with the equilateral triangles composed of gold atoms on both end sulfur atoms at the B3LYP/LANL2DZ level of theory, where we set the Au−Au bond lengths to be 2.88 Å and each sulfur atom is adsorbed on the hollow site. We confirmed from the calculations that the size of the gold clusters does not significantly change the molecular geometry of BDT.

To investigate nonplanarity effects on the transmission, we considered two types of molecular geometries; in one all the benzene rings of the molecules are on a plane (P*n*, $n = 2-5$) and in the other each benzene ring is twisted out of neighboring rings (NP*n*). Figures 4 and 5 show optimized geometries of P*n* and NP*n* at the B3LYP/LANL2DZ level of theory, respectively. For all the PDT molecules, computed Au−S lengths, C−S lengths, and C−S−Au angles are nearly 2.40 Å, 1.84 Å, and 103°, respectively. The nonplanar forms are energetically more stable than the planar ones because the nonplanar forms can reduce the H−H contacts between neighboring benzene rings. The P*n* geometries are not in local minima; there are two, three, three, and four imaginary vibrational modes in P2, P3, P4, and P5, respectively, whereas the NP*n* geometries are in local minima with no imaginary vibrational mode. The energy differences between P*n* and NP*n* are 1.12 kcal/mol in $n = 2$, 2.08 in $n = 3$, 3.01 in $n = 4$, and 3.92 in $n = 5$; that is, the relaxation energy is about 1 kcal/mol per interaction.

Transmission Function of the Benzene 1,4-Dithiolate (BDT) Wire. First, we apply the present method to the molecular junction of BDT coupled with gold electrodes to look at the reliability of the computational procedure. Figure 6 shows a computed transmission function and some MOs of BDT with the P1 conformation. Interesting features obtained are summarized as follows: (1) there is a sharp peak about 2 eV above the Fermi level, and (2) several peaks are broadened below the Fermi level. The present transmission function is similar to those obtained with different methods in previous studies.[23,25]

We see that the MOs of the extended molecule lie in the transmission peak positions. This feature is reasonable considering that the denominator of eq 4 is small near the MO levels. As a result, the zeroth-order Green function elements get large in the vicinity of the MO levels, leading to some remarkable peaks in the transmission function. The magnitude of MO coefficients in the contact region between the molecule and the electrode is also important for the large peaks of the transmission function because large MO coefficients lead to large Green function elements (see eq 4). Taking these points into account, we can rationalize the essential features of the transmission

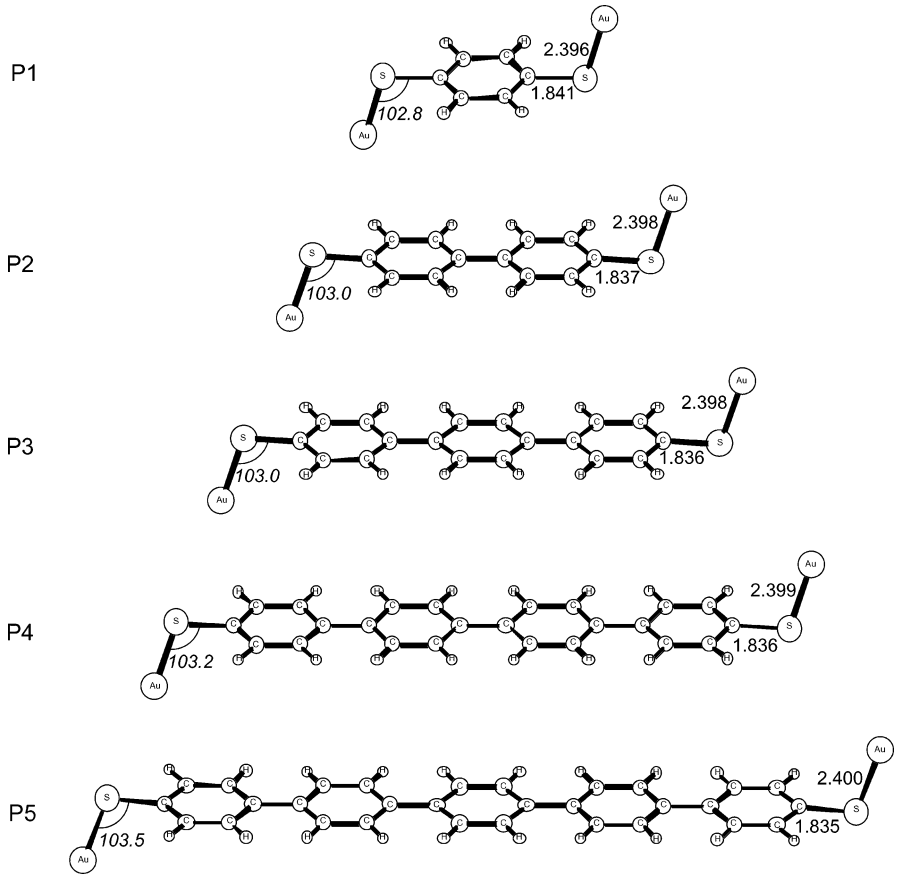

Figure 4. Optimized geometries of P*n* ($n = 1-5$) at the B3LYP/LANL2DZ level of theory. Bond lengths (plain) and bond angles (italic) are in angstroms and degrees, respectively.

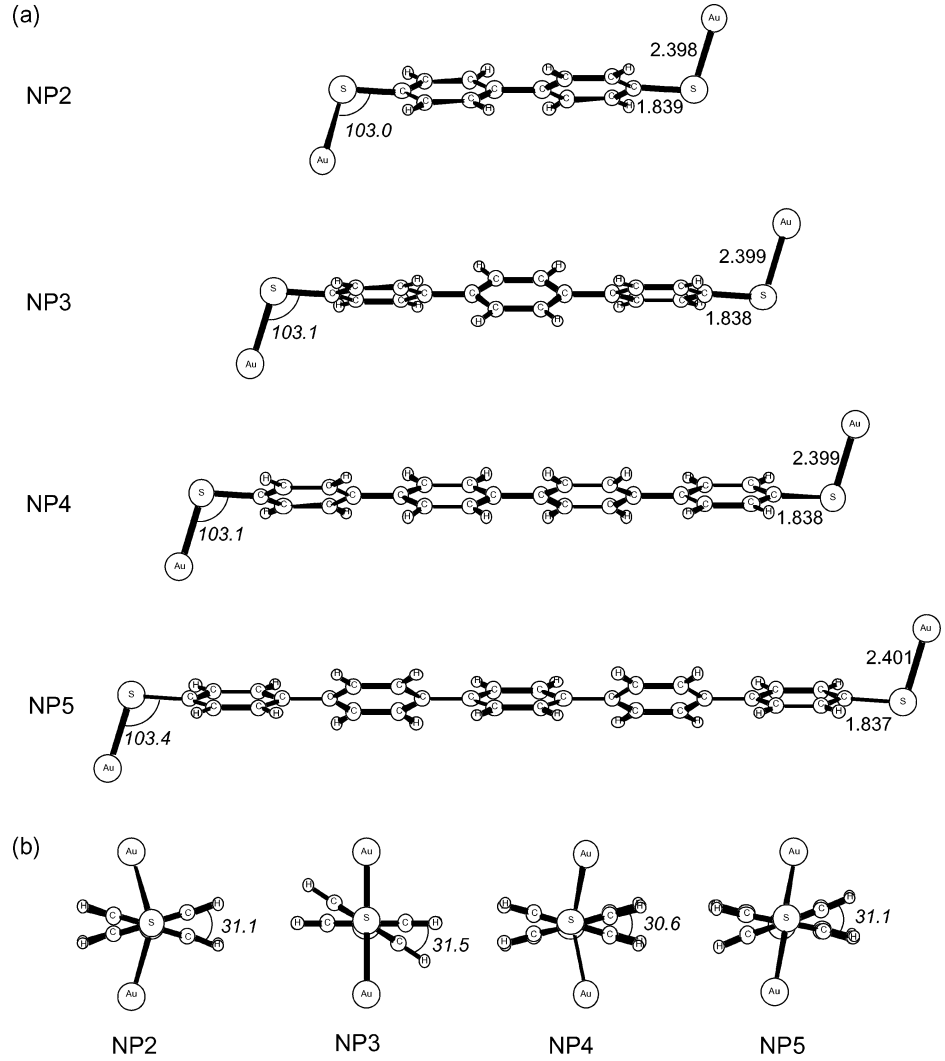

Figure 5. Optimized geometries of NP*n* ($n = 2-5$) at the B3LYP/LANL2DZ of theory. Bond lengths (plain) and bond angles (italic) are in angstroms and degrees, respectively.

function in terms of MOs. The HOMO and LUMO (MOs a and b in Figure 6) are delocalized with large MO coefficients on the sulfur atoms, so the transmission is significantly increased in the vicinity of the HOMO and LUMO. MOs c and d are close in energy, but their contribution to the electrical conduction is different. MO c has large MO coefficients on the sulfur and gold atoms as well as the HOMO and LUMO, and it contributes to the transmission. However, MO d is localized on the benzene ring, and therefore, this orbital does not significantly participate in the transmission. The transmission around -3.6 eV is small because the MOs in this energy region, e.g., MO e, are mainly localized on the two gold atoms.

Transmission Spectra of the Longer Oligo(*p*-phenylene) Dithiolate (PDT) Wires. Let us next look at the conductance of the planar (P*n*) and nonplanar (NP*n*) wires. Figure 7 shows computed transmission spectra of the P*n* and NP*n* ($n = 1-5$) wires. The conductance in the vicinity of the Fermi level is smaller in longer wires except in the P1 wire. Table 1 lists the transmission at the Fermi level. The $T(E_F)$ value of P1 (3.78×10^{-3}) is smaller than those of P2 (7.67×10^{-3}) and NP2 (4.39×10^{-3}). This unusual behavior of P1 is reasonable in view of the HOMOs and LUMOs of PDTs. One can obtain a large transmission function when the product of the MO expansion coefficients on the two atoms connected to electrodes in the HOMO is different in sign from that in the LUMO.[27] However, the MO coefficients on the two sulfur atoms are the same in sign between the HOMO and LUMO of P1 (see Figure 6), so its $T(E_F)$ is small. In contrast, the HOMO and LUMO of P2 satisfy the necessary condition of MO coefficients for large transmission, as shown in Figure 8, and therefore, the transmission function is large (the HOMO and LUMO of NP2 are almost identical to those of P2). The values for the longer wires decay with an increase in wire length, as expected.

Exponential Decay of Transmission in the PDT Wires. A special feature of molecular wires is the exponential decay of conductance. The conductance of molecular wires at low bias voltage is suggested to exponentially decay with an increase in wire length L,[27]

$$G = G_0 e^{-\gamma L} \tag{9}$$

where γ is the damping factor and G_0 is the contact conductance. The γ value is characteristic of molecular wires themselves, and the magnitude of G_0 depends on the adsorption site of wire ends. The exponential decay of conductance has been theoretically investigated and discussed also in refs 46−48. In the present study, we considered the decay of conductance for the PDT system from the viewpoint of MOs. Figure 9 shows the wire-length dependence of the transmission as a function of L, where we define L as the distance between the two sulfur atoms. We estimated from the slopes of the lines the damping factors to be 0.165 and 0.256 Å^{-1} for the P*n* and NP*n* wires,

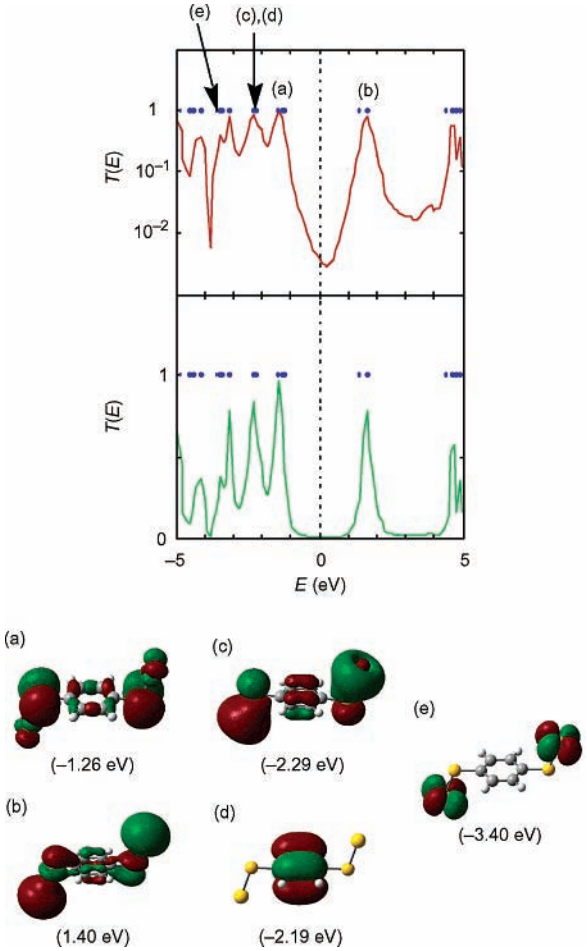

Figure 6. Calculated transmission function and some MOs of BDT (P1 conformation). The transmission is expressed using a log scale (red line) and a linear scale (green line), and blue dots represent the molecular orbital levels (in eV). The Fermi energy of gold is set to zero. MOs a and b are the HOMO and LUMO, respectively.

TABLE 1: Transmission of the PDT Wires at the Femi Level

wire	$T(E_F)$ (planar)	$T(E_F)$ (nonplanar)	nonplanar/planar
PDT1	3.78×10^{-3}		
PDT2	7.67×10^{-3}	4.39×10^{-3}	0.572
PDT3	2.89×10^{-3}	1.39×10^{-3}	0.481
PDT4	1.66×10^{-3}	4.89×10^{-4}	0.295
PDT5	8.43×10^{-4}	1.50×10^{-4}	0.178

respectively, these values being in agreement with a theoretical value of 0.281 $Å^{-1}$ for the PDT wires obtained by Magoga and Joachim.[27] In experimental studies an exponential increase of resistance, $R = R_0 \exp(\beta L)$, was observed in the alkanethiols and oligophenyl self-assembled monolayers (SAMs),[7,9,10] the β values for the oligophenylene SAMs being 0.35−0.5 $Å^{-1}$.[9,10] Kaun et al.[49] obtained values of 0.4−0.51 $Å^{-1}$ using a DFT-based Green function method. Quantity β is essentially identical to the damping factor γ.[17] Thus, the γ values of the PDT wires obtained in the present study are consistent with these theoretical and experimental observations.

Table 1 lists computed values of $T(E_F, \text{NPn})/T(E_F, \text{Pn})$; the ratios for PDT2, PDT3, PDT4, and PDT5 are 0.572, 0.481, 0.295, and 0.178, respectively, which clearly demonstrates that planarity of the π-backbone plays an important role in the quantum transport through longer wires. This feature has a good correlation with the energies of the HOMOs listed in Table 2. The Fermi level of the gold electrodes (−5.31 eV) lies between the HOMOs and LUMOs of all the PDT wires, so one can

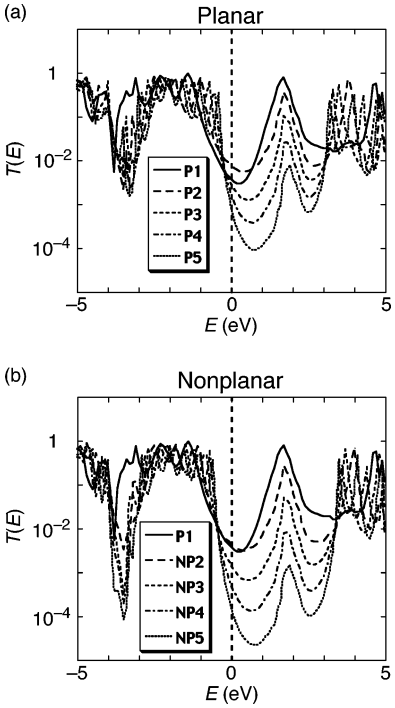

Figure 7. Transmission functions of the PDT wires with (a) planar and (b) nonplanar geometries. The Fermi energy of the gold electrode is set to zero.

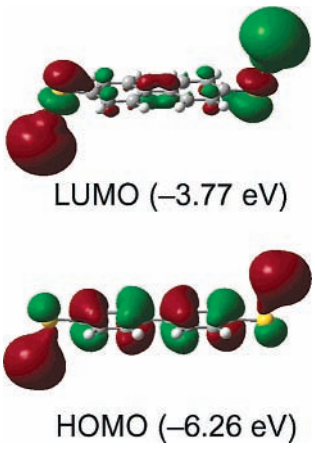

Figure 8. The HOMO and LUMO of the P2 wire.

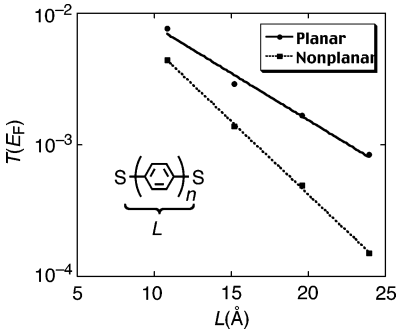

Figure 9. Wire-length dependence of the transmission of the PDT wires. The wire length, L, is defined as the length between the two sulfur atoms. Solid circles and solid squares indicate the transmission of the planar and the nonplanar PDT wires at the Fermi level of electrodes.

expect that both of them should play a role. However, the role of the HOMOs is dominant in the transmission at the Fermi level because the energies of the HOMOs are near the Fermi level in comparison with the LUMOs. Although the LUMOs

TABLE 2: Energies of the HOMOs, LUMOs, and HOMO−LUMO Gaps (in eV) of the PDT Wires (P*n* and NP*n*)[a]

	PDT1	PDT2	PDT3	PDT4	PDT5
			P*n*		
HOMO (eV)	−6.57	−6.26	−6.01	−5.84	−5.72
LUMO (eV)	−3.91	−3.77	−3.69	−3.65	−3.62
HOMO−LUMO gap (eV)	2.66	2.49	2.32	2.19	2.10
			NP*n*		
HOMO (eV)		−6.33 (−0.07)	−6.12 (−0.11)	−5.98 (−0.14)	−5.88 (−0.16)
LUMO (eV)		−3.76 (+0.01)	−3.68 (+0.01)	−3.64 (+0.01)	−3.62 (+0.00)
HOMO−LUMO gap (eV)		2.57 (+0.08)	2.44 (+0.12)	2.34 (+0.15)	2.26 (+0.16)

[a] The values in parentheses are energy differences between P*n* and NP*n*.

remain unchanged in the planar and nonplanar forms, the HOMOs are stabilized in energy and apart from the Fermi level of the gold electrodes in the nonplanar forms. The difference of the HOMO energies in the planar and nonplanar forms increases with an increase in chain length. Therefore, we expect from eq 4 that a large HOMO $- E_F$ energy difference will lead to a small Green function. The significant decrease in conductance of the nonplanar forms is due to the stabilization of the HOMOs of the nonplanar forms.

Concluding Remarks

We have investigated the electrical transmission of some oligo(*p*-phenylene) dithiolate wires coupled with gold electrodes using a Green function method, which is combined with the hybrid density functional method, B3LYP. It provides a reasonable transmission spectrum for the benzene 1,4-dithiolate (BDT) wire. We have also calculated the transmission functions of the longer oligo(*p*-phenylene) dithiolate (PDT) wires with planar and nonplanar forms to look at nonplanarity effects on the electrical transmission through the π-conjugated systems. The conductance (transmission) at the Fermi level exponentially decays with an increase in wire length [$G = G_0 \exp(-\gamma L)$]; the decay is slower in the planar forms than in the nonplanar ones. The damping factors, γ's, for the planar and nonplanar PDT wires are 0.165 and 0.256 Å^{-1}, respectively. These values are comparable with those obtained by other theoretical groups and experimental data for analogous oligophenylene molecules. It is useful to see the HOMOs to understand the calculated results; the location of the HOMOs relative to the Fermi level of the electrodes is an important factor in the difference of the damping factor. Planarity (π-conjugation) is important for effective quantum transport especially in long molecular wires that consist of aromatic rings.

Acknowledgment. K.Y. acknowledges Grants-in-Aid for Scientific Research from the Ministry of Culture, Sports, Science and Technology of Japan (MEXT), Japan Society for the Promotion of Science (JSPS), Japan Science and Technology Cooperation (JST), the Murata Science Foundation, "Nanotechnology Support Project" of MEXT, and Kyushu University P & P "Green Chemistry" for their support of this work. M.K. thanks JSPS for a graduate fellowship.

References and Notes

(1) Joachim, C.; Gimzewski, J. K.; Aviram, A. *Nature* **2000**, *408*, 541.
(2) Carroll, R. L.; Gorman, C. B. *Angew. Chem., Int. Ed.* **2002**, *41*, 4378.
(3) Nitzan, A.; Ratner, M. A. *Science* **2003**, *300*, 1384.
(4) Reed, M. A.; Zhou, C.; Muller, C. J.; Burgin, T. P.; Tour, J. M. *Science* **1997**, *278*, 252.
(5) Reichert, J.; Ochs, R.; Beckmann, D.; Weber, H. B.; Mayor, M.; Löhneysen, H. v. *Phys. Rev. Lett.* **2002**, *88*, 176804.
(6) Weber, H. B.; Reichert, J.; Ochs, R.; Beckmann, D.; Mayor, M.; Löhneysen, H. v. *Physica E* **2003**, *18*, 231.
(7) Bumm, L. A.; Arnold, J. J.; Dunbar, T. D.; Allara, D. L.; Weiss, P. S. *J. Phys. Chem B* **1999**, *103*, 8122.
(8) Cui, X. D.; Primak, A.; Zarate, X.; Tomfohr, J.; Sankey, O. F.; Moore, A. L.; Moore, T. A.; Gust, D.; Harris, G.; Lindsay, S. M. *Science* **2001**, *294*, 571.
(9) Wold, D. J.; Haag, R.; Rampi, M. A.; Frisbie, C. D. *J. Phys. Chem. B* **2002**, *106*, 2813.
(10) Ishida, T.; Mizutani, W.; Aya, Y.; Ogiso, H.; Sasaki, S.; Tokumoto, H. *J. Phys. Chem. B* **2002**, *106*, 5886.
(11) Xue, Y.; Datta, S.; Ratner, M. A. *J. Chem. Phys.* **2001**, *115*, 4292.
(12) Damle, P. S.; Ghosh, A. W.; Datta, S. *Phys. Rev. B* **2001**, *64*, 201403.
(13) Palacios, J. J.; Pérez-Jiménez, A. J.; Louis, E.; Vergés, J. A. *Phys. Rev. B* **2001**, *64*, 115411.
(14) Palacios, J. J.; Pérez-Jiménez, A. J.; Louis, E.; SanFabián, E.; Vergés, J. A. *Phys. Rev. B* **2002**, *66*, 35322.
(15) Taylor, J.; Guo, H.; Wang, J. *Phys. Rev. B* **2001**, *63*, 245407.
(16) Brandbyge, M.; Mozos, J.-L.; Ordejón, P.; Taylor, J.; Stokbro, K. *Phys. Rev. B* **2002**, *65*, 165401.
(17) Samanta, M. P.; Tian, W.; Datta, S.; Henderson, J. I.; Kubiak, C. P. *Phys. Rev. B* **1996**, *53*, R7626.
(18) Emberly, E. G.; Kirczenow, G. *Phys. Rev. B* **1998**, *58*, 10911.
(19) Yaliraki, S. N.; Roitberg, A. E.; Gonzalez, C.; Mujica, V.; Ratner, M. A. *J. Chem. Phys.* **1999**, *111*, 6997.
(20) Hall, L. E.; Reimers, J. R.; Hush, N. S.; Silverbrook, K. *J. Chem. Phys.* **2000**, *112*, 1510.
(21) Di Ventra, M.; Pantelides, S. T.; Lang, N. D. *Phys. Rev. Lett.* **2000**, *84*, 979.
(22) Wang, C.-K.; Fu, Y.; Luo, Y. *Phys. Chem. Chem. Phys.* **2001**, *3*, 5017.
(23) Derosa, P. A.; Seminario, J. M. *J. Phys. Chem. B* **2001**, *105*, 471.
(24) Stokbro, K.; Taylor, J.; Brandbyge, M.; Mozos, J.-L.; Ordejón, P. *Comput. Mater. Sci.* **2003**, *27*, 151.
(25) Chen, H.; Lu, J. Q.; Wu, J.; Note, R.; Mizuseki, H.; Kawazoe, Y. *Phys. Rev. B* **2003**, *67*, 113408.
(26) (a) Xue, Y.; Ratner, M. A. *Phys. Rev. B* **2003**, *68*, 115406. (b) Xue, Y.; Ratner, M. A. *Phys. Rev. B* **2003**, *68*, 115407.
(27) Magoga, M.; Joachim, C. *Phys. Rev. B* **1997**, *56*, 4722.
(28) Tada, T.; Yoshizawa, K. *ChemPhysChem* **2002**, *3*, 1035.
(29) Tada, T.; Yoshizawa, K. *J. Phys. Chem. B* **2003**, *107*, 8789.
(30) Priyadarshy, S.; Skourtis, S. S.; Risser, S. M.; Beratan, D. N. *J. Chem. Phys.* **1996**, *104*, 9473.
(31) Datta, S. *Electronic Transport in Mesoscopic Systems*; Cambridge University Press: Cambridge, 1995.
(32) Heurich, J.; Cuevas, J. C.; Wenzel, W.; Schön, G. *Phys. Rev. Lett.* **2002**, *88*, 256803.
(33) Becke, A. D. *J. Chem. Phys.* **1993**, *98*, 5648.
(34) Stephens, P. J.; Devlin, F. J.; Chabalowski, C. F.; Frisch, M. J. *J. Phys. Chem.* **1994**, *98*, 11623.
(35) Dunning, T. H., Jr.; Hay, P. J. In *Modern Theoretical Chemistry*; Schaefer, H. F., III, Ed.; Plenum: New York, 1976; Vol. 3, p 1.
(36) (a) Wadt, W. R.; Hay, P. J. *J. Chem. Phys.* **1985**, *82*, 284. (b) Hay, P. J.; Wadt, W. R. *J. Chem. Phys.* **1985**, *82*, 299.
(37) Frisch, M. J.; Trucks, G. W.; Schlegel, H. B.; Scuseria, G. E.; Robb, M. A.; Cheeseman, J. R.; Zakrzewski, V. G.; Montgomery, J. A., Jr.; Stratmann, R. E.; Burant, J. C.; Dapprich, S.; Millam, J. M.; Daniels, A. D.; Kudin, K. N.; Strain, M. C.; Farkas, O.; Tomasi, J.; Barone, V.; Cossi, M.; Cammi, R.; Mennucci, B.; Pomelli, C.; Adamo, C.; Clifford, S.; Ochterski, J.; Petersson, G. A.; Ayala, P. Y.; Cui, Q.; Morokuma, K.; Malick, D. K.; Rabuck, A. D.; Raghavachari, K.; Foresman, J. B.; Cioslowski, J.; Ortiz, J. V.; Stefanov, B. B.; Liu, G.; Liashenko, A.; Piskorz, P.; Komaromi, I.; Gomperts, R.; Martin, R. L.; Fox, D. J.; Keith, T.; Al-Laham, M. A.; Peng, C. Y.; Nanayakkara, A.; Gonzalez, C.; Challacombe, M.; Gill, P. M. W.; Johnson, B. G.; Chen, W.; Wong, M. W.; Andres, J. L.; Head-Gordon, M.; Replogle, E. S.; Pople, J. A. *Gaussian 98*; Gaussian, Inc.: Pittsburgh, PA, 1998.
(38) Hoffmann, R. *J. Chem. Phys.* **1963**, *39*, 1397.

(39) Landrum, G. A.; Glassey, W. V. *YAeHMOP: Yet Another Extended Hückel Molecular Orbital Package*; Cornell University: Ithaca, NY, 1995; http://sourceforge.net/projects/yaehmop/.

(40) Guinea, F.; Tejedor, C.; Flores, F.; Louis, E. *Phys. Rev. B* **1983**, *28*, 4397.

(41) López Sancho, M. P.; López Sancho, J. M.; Rubio, J. *J. Phys. F* **1985**, *15*, 851.

(42) Slater, J. C.; Koster, G. F. *Phys. Rev.* **1954**, *94*, 1498.

(43) Papaconstantopoulos, D. A. *Handbook of the Band Structure of Elemental Solids*; Plenum: New York, 1986.

(44) *CRC Handbook of Chemistry and Physics*; Lide, D. R., Ed.; CRC Press: Boca Raton, FL, 2000; Chapter 12, p 130.

(45) We have applied the present computational procedure to an alkanethiolate system and estimated the damping factor. The calculated damping factor was 0.679 $Å^{-1}$, which is comparable with the value in ref 9 (0.94 $Å^{-1}$).

(46) Magoga, M.; Joachim, C. *Phys. Rev. B* **1998**, *57*, 1820.

(47) Tomfohr, J. K.; Sankey, O. F. *Phys. Rev. B* **2002**, *65*, 245105.

(48) Xue, Y.; Ratner, M. A. *Appl. Phys. Lett.* **2003**, *83*, 2429.

(49) Kaun, C.-C.; Larade, B.; Guo, H. *Phys. Rev. B* **2003**, *67*, 121411.